Available online at www.sciencedirect.com
ScienceDirect
Ceramics International 35 (2009) 315–320
CERAMICS INTERNATIONAL
www.elsevier.com/locate/ceramint

Defect analysis of Y^{3+}-doped $Ba_{0.95}Sr_{0.05}Ti_{1-x}O_{3-\delta}$ above Curie temperature

S. Suasmoro *, E. Hastuti, D. Darminto

Department of Physics, Faculty of Mathematics and Sciences, Institute of Technology 'Sepuluh Nopember' Surabaya Kampus ITS Sukolilo, Surabaya 60111, Indonesia

Received 5 September 2006; received in revised form 20 September 2007; accepted 22 October 2007
Available online 16 January 2008

Abstract

Several possible defect structures in $Ba_{0.95}Sr_{0.05}TiO_3$-doped with 0, 0.2, 0.4 and 0.6% molar of Y^{3+} have been analyzed. Polycrystalline samples used in this study were synthesized via an oxalate coprecipitation technique, subsequently followed by calcination at 700 °C for 2 h and sintering at 1300 °C for 2 h. Structural and microstructural characterizations using XRD and SEM show a slight decrease of lattice tetragonality (c/a) and densification with increasing Y^{3+} content up to 0.4%. Electrical measurements were conducted by applying an alternating electric field of 15 V/cm with the frequency range between 50 Hz and 1 MHz at elevated temperature from room temperature up to 300 °C in air. We have noted three phenomena with respect to the characteristics of dielectric constant exhibited by the samples, namely a structural transition from tetragonal to cubic at Curie temperature, the high frequency as well as low frequency relaxation processes occurring respectively at $T \approx 180$ °C and $T \approx 250$ °C. Further analysis by the Cole–Cole plot of dielectric constant and complex impedance has suggested the main cause of the related features to be pair defects as $V_{Ti}''' - V_O^{\bullet\bullet}$ and $V_{Ba}'' - V_O^{\bullet\bullet}$.

Keywords: B. Defects; C. Ferroelectric; C. Dielectric; C. Impedance; C. Conductivity; Oxygen diffusion

1. Introduction

Ferroelectrics $BaTiO_3$ is one of the materials extensively studied due to its wide use in electronics, e.g.: multilayer ceramics capacitor (MLCC), positive temperature coefficient resistors (PTCR) and many others [1–3]. Numerous contributions have been focused on the effect of doping on crystal structure, defect structure and electrical properties [4–6]. There are two types of substitutions for cation doping of the compound which is commonly classified as perovskite or ABX_3 system. The first type is a larger dodecahedral A sites substitution for ions such as La^{3+}, Ce^{3+}, Sr^{2+}. The second type is a smaller octahedral B sites substitution, especially for ions such as Nb^{5+}, Sb^{5+}, Al^{3+} [5–8]. Meanwhile, Y^{3+} can be incorporated in either A or B site, as its ionic radius is in between those of Ba^{2+} and Ti^{4+}.

Zhi et al. [9], studied the incorporation of Y^{3+} in $BaTiO_3$ using XRD. It was shown that Y^{3+} substituting Ba^{2+} at A sites has induced a formation of Ti vacancy to lead to a composition of $(Ba_{1-x}Y_x)Ti_{1-x/4}(Ti)_{x/4}O_3$ ($x < 0.015$). Further, when Y^{3+} substituted Ti^{4+} at B sites, an oxygen vacancy was created to be associated with a composition of $BaTi_{1-y}Y_yO_{3-\delta}$ ($y < 0.059$). Additionally, Ho^{3+} and Dy^{3+} were also operative to yield the same effects [10].

The undoped $BaTiO_3$ is electrically insulating. It becomes semiconducting at high temperature (>1350 °C) or in a reduced atmosphere, since the intrinsic defects of $V_O^{\bullet\bullet}$ and e' are formed by releasing oxygen. It has been well understood that the doped $BaTiO_3$ is n-type semiconductor in very low oxygen pressure. It switches to be p-type semiconductor when the oxygen pressure is applied to be more than 10^{-5} Pa at relatively high temperature (>800 °C) [11]. Moreover, a cation incorporation in the crystal will lead to the structure rearrangement and consequently other properties are therefore modified. Zhang et al. [12] showed that the dielectric type curve of $BaTiO_3$ became a relaxor because of Nb^{5+} substitution. The equivalent effect was also observed on doped paraelectric $SrTiO_3$ [13].

Studies on solubility of Y^{3+} in $Ba_{0.95}Sr_{0.5}Ti_{1-x}O_{3-\delta}$ using XRD and WDS techniques have also been conducted [9,10].

* Corresponding author.
E-mail address: suasm@its.ac.id (S. Suasmoro).

0272-8842/$34.00
doi:10.1016/j.ceramint.2007.10.011

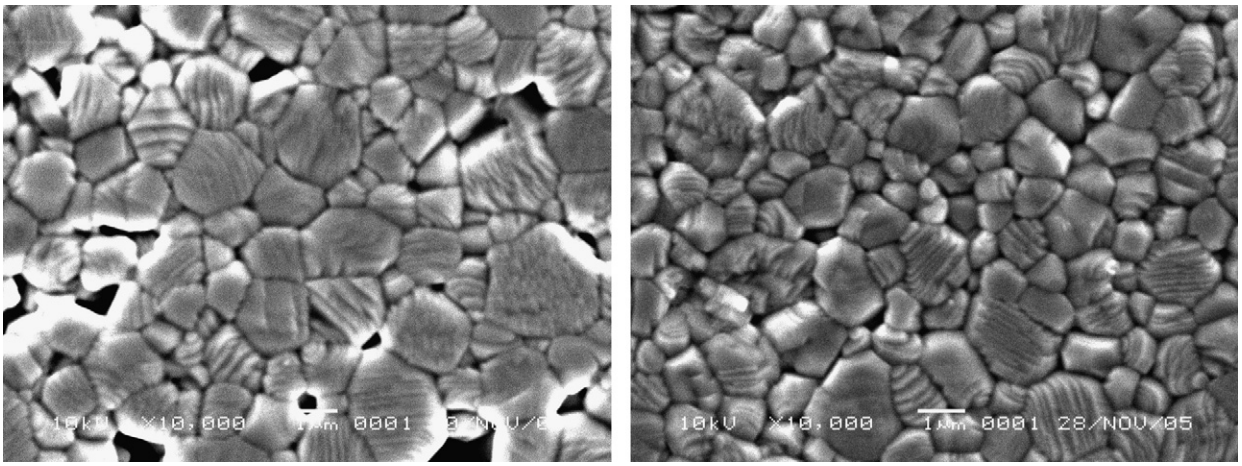

Fig. 1. SEM images of thermally etched undoped (left) and 0.4% Y^{3+}-doped (right) $Ba_{0.95}Sr_{0.05}TiO_3$.

The solid solution of Y^{3+}-doped $Ba_{0.95}Sr_{0.5}Ti_{1-x}O_{3-\delta}$ has been examined as regards its structure, dielectric properties and impedance. Cole–Cole plot of dielectric constant and impedance analyses were carried out in conjunction with the electric response to investigate the type of defects in the sample. However, as reported by Zhang et al. [12] and Ang et al. [13], such investigations were carried out in a relatively low temperature range, starting from room temperature and up to 300 °C and focused on phenomena above T_c. To our best knowledge, a further study on this phenomenon which is especially related to pair defects has not so far been reported.

2. Experimental

Reagent grade raw materials consisting of $TiCl_4$, $BaCl_2{\cdot}2H_2O$, $SrCl_2{\cdot}2H_2O$ and $H_2C_2O_4{\cdot}2H_2O$ (E. Merck) were used to synthesize (Ba/Sr)$TiO(C_2O_4)_2{\cdot}4H_2O$ precursor through an oxalate coprecipitation technique as described elsewhere [14]. The precursor was then calcined at 700 °C for 2 h and examined their stochiometry to obtain a ratio of (Ba + Sr)/Ti being slightly higher than one [15]. Y_2O_3 as dopant was added to the calcined powder with the ratio of 0, 0.2, 0.4 and 0.6% molar fraction. The mixture was ground using a planetary milling and ethanol as milling media. Green pellet was obtained by pressing the mixed powder using an isostatic die with a disc shape having diameter of 13 mm and thickness of ∼1.5 mm. The pellet was finally sintered in air at 1300 °C for 2 h.

Characterizations of the samples include analyses of microstructure and structure, measurements of permittivity as well as impedance, using SEM (JEOL JSM-6360), XRD (Phillip X'Pert MPD) with Cu Kα X-ray radiation and an electrical measuring apparatus (RCL-Fluke PM6306). The XRD data were taken at room temperature with 0.02° acquisition step, and analyzed by Rietveld refinement [16]. Permittivity and impedance characterizations were conducted by applying an alternating electric field of 15 V/cm in the frequency range of 50 Hz to 1 MHz. During the measurements, samples were placed in the center of a tubular furnace at temperature starting from room temperature up to 300 °C in air, and in the temperature range between 300 °C and 500 °C in a controlled oxygen atmosphere. The electrical data were further analyzed by Cole–Cole plot to evaluate permittivity and conductivity.

3. Results and discussion

3.1. Structure and microstructure characterization

Structural and microstructural properties of the ceramics, such as density, grain size, and lattice parameters were studied. The SEM images in Fig. 1 show a typical micrograph of the examined samples. It can be seen that the grains are typically rounded with sub-micron average grain size. The grains are seen to be multilayer, which is obviously identified as ferroelectric domains. The XRD analysis of crushed sintered sample depicted in Fig. 2 shows a single-phase diffraction pattern. This indicates that Y^{3+} is incorporated in A/B sites. The spectra for the doped samples are precisely similar with a slight shift of the diffraction peak positions and modified intensity patterns (inset to Fig. 2).

For more detailed analysis, Rietveld refinements have been carried out to evaluate the lattice parameters. For all the samples, the 'figure of merit' *R*-factor is in the range for accepted refinement as proposed by Kisi [17]. The results of structure and microstructure analyses are collected in Table 1. It can be singled

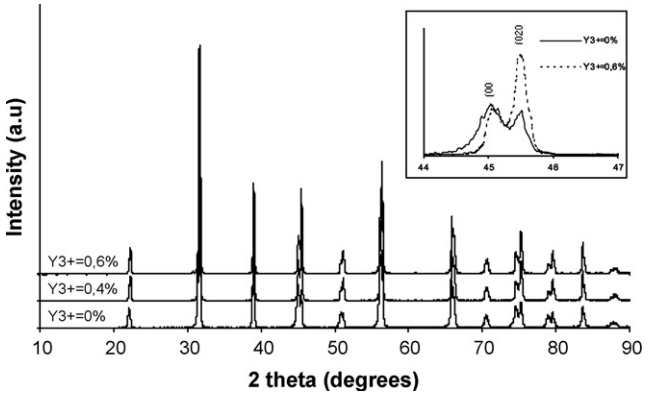

Fig. 2. XRD pattern of Y^{3+}-doped $Ba_{0.95}Sr_{0.05}TiO_3$. Inset: the shift and change of the diffraction peaks (0 0 2) and (0 2 0) reflection planes.

Table 1
Microstructure and structure parameter of Y^{3+}-doped $Ba_{0.95}Sr_{0.05}TiO_3$

Y^{3+} (mol.%)	Relative density (%)	Average grain size (μm)	Lattice parameter (Å)		
			a	*c*	*c*/*a*
0	86 ± 1	0.99 ± 0.05	3.99455 ± 0.00005	4.03089 ± 0.00001	1.00909
0.02	90 ± 1	0.91 ± 0.05	–	–	–
0.04	93 ± 2	0.47 ± 0.06	3.99525 ± 0.00005	4.02853 ± 0.00003	1.00833
0.06	92 ± 1	0.49 ± 0.05	3.99423 ± 0.00003	4.02799 ± 0.00001	1.00845

out that Y^{3+} improves densification and causes reduction of grain growth. Moreover, these mentioned effects seem to be optimized at the doping level up to 0.4%. The obtained lattice parameters exhibit a tetragonal structure for all samples and, on the other hand, their *c*-axis lengths slightly shrink with increasing doping level. The alternate figure for the *a*-axis in this doping range disagrees with the literatures [9,10] results, where it should linearly expand with increasing doping concentration.

3.2. Electrical characterization

Results of dielectric constant of Y^{3+}-doped $Ba_{0.95}Sr_{0.05}TiO_3$ measured at elevated temperatures up to 300 °C in air are depicted in Fig. 3. For the undoped sample, three phenomena in the dependency of dielectric constant on temperatures and frequencies have been noted, i.e.: (i) mode A occurring at $T \sim 120$ °C is the well known phase transition from tetragonal to cubic related to Curie temperature point; (ii) mode B which takes place only at high frequency (> 100 KHz) at $T \sim 180$ °C; (iii) mode C occurring at $T \sim 250$ °C at low frequency (<1 KHz). The last two phenomena are operative at $T > T_c$, and they are therefore considered to be unrelated to the structural transition. Further feature can be marked in this characteristic; when the sample thickness is reduced, the signal modes get weaker especially in the high frequency part.

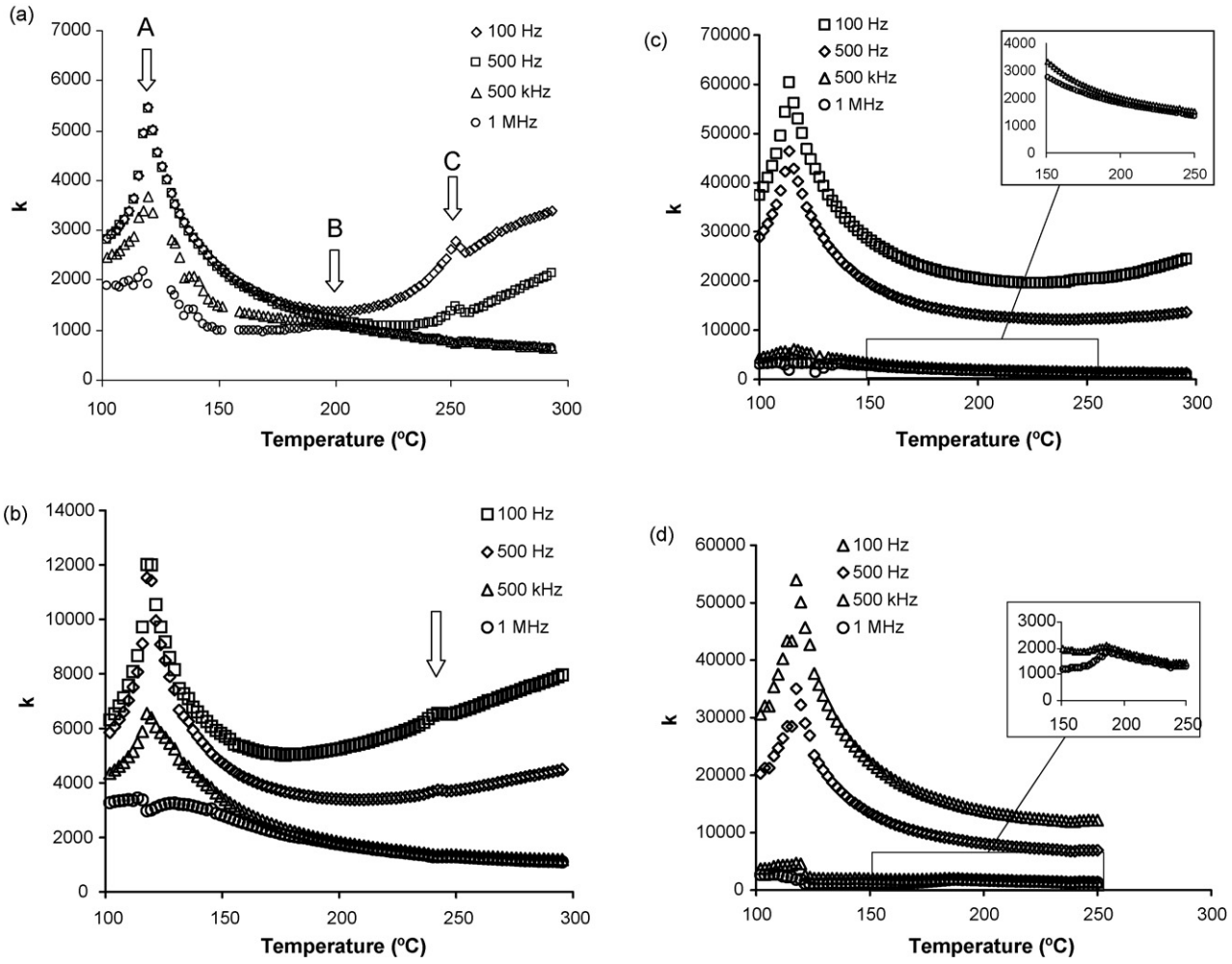

Fig. 3. The dependencies of dielectric constant *k* of Y^{3+}-doped $Ba_{0.95}Sr_{0.05}TiO_3$ on temperature: (a) 0%; (b) 0.02%; (c) 0.04%; (d) 0.06%.

For the doped samples with $Y^{3+} = 0.2\%$, the modes B disappear; however, the modes C still persist. For further increasing doping level up to 0.4%, both modes B and C disappear. The characteristics of dielectric constant of these samples exhibit a normal curve, and for $Y^{3+} = 0.6\%$ the modes C reappear. Recalling that in this specific sample, the ionic ratio (Ba + Sr)/Ti of the undoped $Ba_{0.95}Sr_{0.05}TiO_3$ is slightly higher than one; and this compound should consequently have the formula of $Ba_{0.95}Sr_{0.05}Ti_{1-x(Ti)}{}_xO_{3-\delta}$. When the temperature is increased, intrinsic V''_{Ba} and $V_O^{\bullet\bullet}$ Schottky defects are formed, in addition to the pre-existence of V''''_{Ti}. From this point of view, the relaxation is related to the presence of defects, where the modes B should be attributed by the environment of a smaller cationic vacancy V''''_{Ti}, and the modes C should be attributed by the environment of a larger cationic vacancy V''_{Ba}. In this regard, the resulting pair defects of $V''''_{Ti} - V_O^{\bullet\bullet}$ and $V''_{Ba} - V_O^{\bullet\bullet}$ should stand as dipoles. A similar feature has been reported in Bi-doped $SrTiO_3$ [18].

The disappearance of modes B because of Y^{3+} incorporation indicates that the vacant Ti sites are occupied by the ions to form Y'_{Ti}, and consequently, the dipole $V''''_{Ti} - V_O^{\bullet\bullet}$ no longer exists. When Y'_{Ti} is saturated with increasing doping level, Y^{3+} begins to incorporate in the V''_{Ba} site to form $Y_{Ba}^{\bullet}$. This leads to the disappearance of modes C and therefore $V''_{Ba} - V_O^{\bullet\bullet}$ dipole. Further increase in doping concentration should induce the formation of $Y_{Ba}^{\bullet}$ and force the creation of V''''_{Ti}, rendering consequently the dipole $V''''_{Ti} - V_O^{\bullet\bullet}$ to reappear.

The following analysis will focus on the electrical properties of the samples. The Cole–Cole plots of dielectric constant k'–k'' have been given in Fig. 4. It can be noted that the undoped sample has one semicircle with radius of ~1100. The 0.2% doped sample has similar feature than the undoped sample and shows small queue having radius of ~1700. The 0.4% and 0.6% doped-samples show two semicircles: the high frequency part having radius of ~1900 and ~1500, and the low frequency part having radius of ~10,500 and ~8700. The high frequency semicircle in the Cole–Cole plot should suggest an occurrence of polarization due to permanent lattice dipole. The increase of semicircle radius of the doped samples is due to additional dipole induced by a space charge, which stands a granular dipole under alternating electric field through trapping and de-trapping mechanism at the grain boundaries. The decrease of semicircle radius of 0.6% doped sample indicates a decrease of dipole density *a priori* caused by losses. The large semicircle at low frequency part for the 0.4% and 0.6% doped samples are attributed by a long-range bulk dipole originated from the space charge.

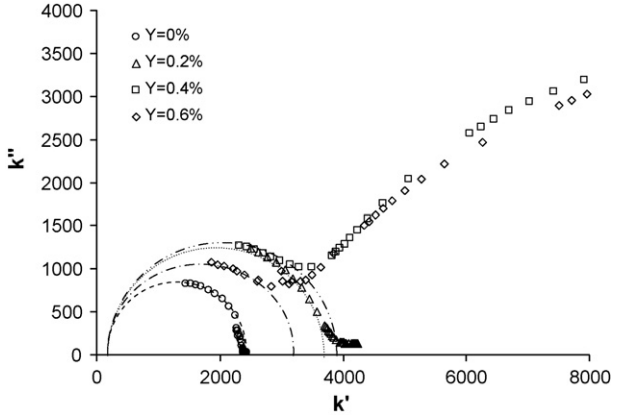

Fig. 4. Cole–Cole plot of Y^{3+}-doped $Ba_{0.95}Sr_{0.05}TiO_3$.

The conductivity of samples were deduced from the diameter of Cole–Cole plot of complex impedance analysis using the model describing a serial circuit of two parallel loops [5]: the first loop consisting of resistance and capacitance arising from the grains, and the second loop covering resistance and capacitance of the grain boundaries as given in Fig. 5. The figures exhibit similar trend of $\ln \sigma$ versus $1/T$ curves. In the range of evaluated temperatures, it is shown that the 0.6% Y^{3+}-doped sample has higher conductivity compared to that of undoped sample, and this explains the existence of space charge on the doped sample. There are two phenomena for bulk response which can be distinguished as follows; the PTCR effect which is associated with a relaxation on modes A and B, and a non-linear relation in Arrhenius plot below T_c. In the latter phenomenon, the characteristics is similar to that of the empirical Vogel–Fulcher law, as modified Archenius law, in time constant of relaxation [13]. Besides, the grain response exhibits two regions in normal Arrhenius plot, namely below T_c and above the modes B.

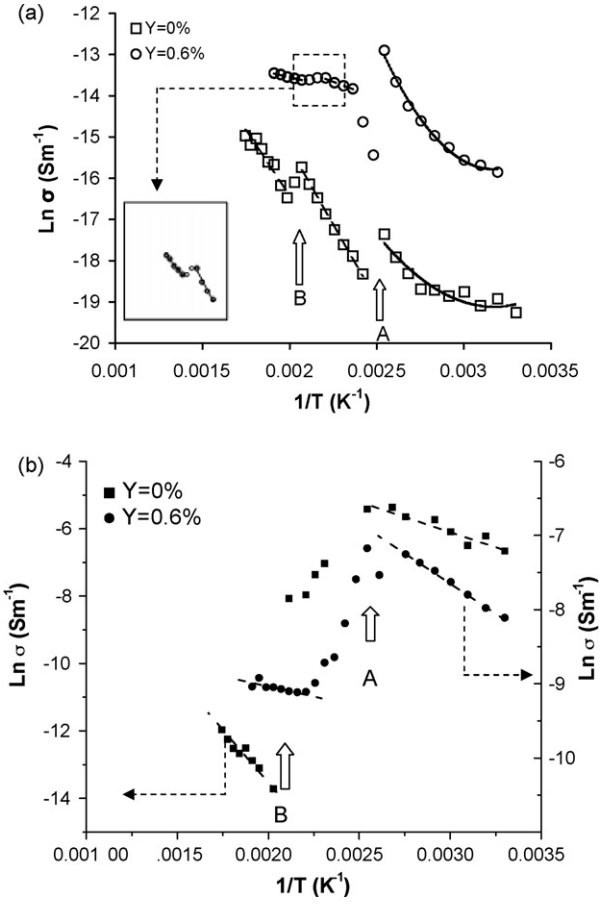

Fig. 5. Plot of temperature dependence of conductivity for undoped and 0.6% Y^{3+}-doped $Ba_{0.95}Sr_{0.05}TiO_3$. (a) Bulk conductivity (b) Grain conductivity.

Table 2
Activation energy of Y^{3+}-doped $Ba_{0.95}Sr_{0.05}TiO_3$ determined from conduction curves

Y^{3+} (mol.%)	Bulk		Grain	
	ΔE (eV)[a]	ΔE (eV)[b]	ΔE (eV)[b]	ΔE (eV)[c]
0	0.63 ± 0.02	0.53 ± 0.06	0.48 ± 0.05	0.15 ± 0.02
0.2	¶	0.16 ± 0.01	0.49 ± 0.03	0.13 ± 0.03
0.4	¶	0.29 ± 0.03	0.68 ± 0.07	0.19 ± 0.01
0.6	0.14 ± 0.02	0.09 ± 0.01	0.06 ± 0.01	0.14 ± 0.01

¶No modes are detected above T_c.
[a] between modes A and B.
[b] above mode B.
[c] below mode A.

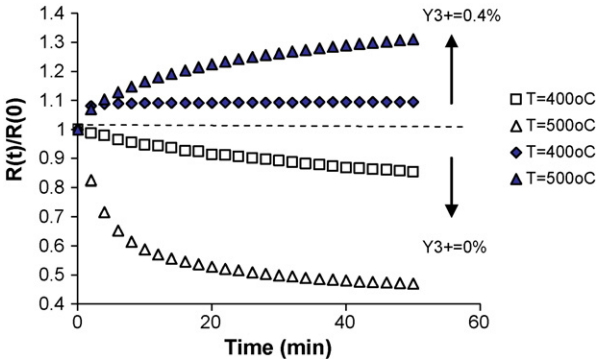

Fig. 6. The evolution of relative resistance during oxygen diffusion in the sample measured at the frequency 500 Hz.

The activation energy of electrical conduction process extracted from the Arrhenius law is presented in Table 2. It shows that for the bulk case the activation energy is lower for the doped samples, indicating that the dopant affects the grain boundary layer. In contrast, the grain conductivity has high activation energy for 0.4% doped sample. This last result emphasizes the explanation given for the permittivity characteristics, where Y^{3+} occupies $V_{Ti}^{''''}$ and $V_{Ba}^{''}$ in this doping level. The lowest activation energy for 0.6% doped sample is reasonably attributed by electron donors having energy state near the conduction band, which takes a role as space charge.

3.3. Oxygen diffusion

In the discussion described above, the oxygen vacancy $V_O^{\bullet\bullet}$ exists in all cases. To further verify this matter, the oxygen diffusion experiments were performed in the temperature range of 300–500 °C and the results are given in Fig. 6. Samples were initially homogenized at 650 °C in a flowing nitrogen atmosphere for 1 h, then the temperature is set down to the desired temperature and the atmosphere is suddenly switched from nitrogen to oxygen. When the oxygen is diffused into the sample, the doped sample becomes more conductive, while the undoped sample becomes more resistive. To explain this different response, one can consider that as soon as the oxygen is diffused in the doped sample, $V_O^{\bullet\bullet}$ becomes O_O^x, implying a reduction of space charge and, as a result, the decrease of the number of charge carrier. Meanwhile, the diffused oxygen consequently suppresses the creation of $V_{Ba}^{''}$ for the undoped sample.

4. Conclusions

The investigation of Y^{3+}-doped $Ba_{0.95}Sr_{0.05}TiO_3$ ferroelectric ceramics through analyses covering the structure and microstructure, the dielectric constant, Cole–Cole plot of permittivity and complex impedance has been carried out. The incorporation of Y^{3+} in $Ba_{0.95}Sr_{0.05}TiO_3$ has led to slightly reduced lattice tetragonality (c/a) and densification for the doping level of Y^{3+} up to 0.4%. The phenomena of high frequency relaxation at $T \approx 180$ °C and the low frequency relaxation at $T \approx 250$ °C are predicted to be attributed by the environment of smaller defect $V_{Ti}^{''''}$ due to non-stoichiometric composition and larger defect $V_{Ba}^{''}$ caused by intrinsic defect at elevated temperatures. These two type defects together with $V_O^{\bullet\bullet}$ neutralization have created pair defects which stand as $V_{Ti}^{''''} - V_O^{\bullet\bullet}$ and $V_{Ba}^{''} - V_O^{\bullet\bullet}$ dipoles. When Y^{3+} occupies the vacancies of titanium and barium, the relaxation phenomena disappear and grain conductivity with a high activation energy set in. The oxygen insertion in $V_O^{\bullet\bullet}$ reduces the amount of space charge for the undoped sample, while suppresses $V_{Ba}^{''}$ creation for the doped samples.

Acknowledgements

This work was supported by the Indonesian State Ministry of Research and Technology through 'RUT-IX' program under contract No:23/Perj/DepIII/RUT/PPKI/II/2005. The authors thank to Malik Anjelh Baqiya for his help in data acquisition for the experiment of oxygen diffusion.

References

[1] S.H. Yoon, K.H. Lee, H. Kim, Effect on the segregation of donors in niobium-doped barium titanate positive temperature Coefficient Resistors, J. Am. Ceram. Soc. 83 (10) (2000) 2463–2472.
[2] Q. Feng, C.J. McConville, D.D. Edwards, Dielectric Properties and microstructure of Ba(Ti, Zr)O_3, J. Am. Ceram. Soc. 88 (6) (2005) 1455–1460.
[3] N.S. Hari, T.R.N. Kutty, Effect of secondary-phase segregation on the positive temperature coefficient in resistance characteristics of n-$BaTiO_3$ ceramics, J. Mater. Sci. (1988) 3284–233275.
[4] H. Pinto, A. Stashans, P. Sanchez, Theoretical studies of impurity doped and undoped $BaTiO_3$, Nato Sci. Ser., High Technol. 77 (2000) 67–72.
[5] O. Kamishima, Y. Abe, T. Ishii, J. Kawamura, T. Hatori, Dielectric relaxation in Yb-doped $SrZrO_3$, J. Phys. Condens. Mater. 16 (2004) 4871–4981.
[6] I.J. Clark, F.B. Marques, D.C. Sinclair, The influence of grain boundaryimpedances on the p-type conductivity of undoped $BaTiO_3$, J. Eur. Ceram. Soc. 22 (2002) 579–583.
[7] F.D. Morison, D.C. Sinclair, A.R. West, Characterization of lanthanum-doped barium titanate ceramics using impedance spectroscopy, J. Am. Ceram. Soc. 84 (3) (2001) 531–538.
[8] Q. Jianquan, C. Wanping, Z. Zhongtai, T. Zilong, Acceptor compensation in (Sb, Y)-doped semiconducting $Ba_{1-x}Sr_xTiO_3$, J. Mater. Sci. 32 (1997) 713–717.
[9] J. Zhi, A. Chen, Y. Zhi, P.M. Vilarinko, J.L. Baptista, Incorporation of yttrium in barium titanate ceramics, J. Am. Ceram. Soc. 82 (5) (1999) 1345–1348.

[10] D. Makovec, Z. Samardžija, M. Drofenik, Solid solubility of holmium, yttrium, and dysprosium in $BaTiO_3$, J. Am. Ceram. Soc. 87 (7) (2004) 1324–1329.
[11] C.R. Song, H.I. Yoo, Chemical diffusivity of $BaTiO_{3-\delta}$: IV acceptor-doped case, J. Am. Ceram. Soc. 83 (4) (2000) 773–779.
[12] R. Zhang, J.F. Li, D. Viehland, Effect of Aliovalent substitutions on the ferroelectric properties of modified barium titanate ceramics: relaxor ferroelectric behavior, J. Am. Ceram. Soc. 87 (5) (2004) 864–870.
[13] C. Ang, Z. Jing, Z. Yu, Ferroelectric relaxor $Ba(TiCe)O_3$, J. Phys. Condens. Mater. 14 (2002) 8901–8912.
[14] Bernier, J.C., Poix, P.J.L., Rhespringer, French Patent 2,570,373, September 18, 1986.
[15] S. Suasmoro, S. Pratapa, D. Hartanto, D. Setyoko, U.M. Dani, The characterization of mixed titanate $Ba_{1-x}Sr_xTiO_3$ phase formation from oxalate coprecipitated precursors, J. Eur. Ceram. Soc. 20 (2000) 309–314.
[16] Hunter, B.A., 'Rietica', in Newsletter of International Union of Crystallography, Commission on Powder Diffraction, 20, Sydney, p. 21.
[17] E.H. Kisi, Rietveld analysis of powder diffraction patterns, Mater. Forum 18 (1994) 135–153.
[18] C. Ang, Z. Yu, Dielectric relaxor and ferroelectric relaxor: Bi-doped paraelectric $SrTiO_3$, J. Appl. Phys. 91 (13) (2002) 1487–1494.